Miner Deposita (2006) 41: 357–368
DOI 10.1007/s00126-006-0064-8

ARTICLE

D. Craw

Pressure-oxidation autoclave as an analogue for acid–sulphate alteration in epithermal systems

Received: 2 November 2005 / Accepted: 11 April 2006 / Published online: 18 May 2006

Abstract Gold extraction at the Macraes gold mine in New Zealand involves concentration of pyrite and arsenopyrite, oxidation of those sulphides, then cyanidation. The ore concentrate is predominantly Otago Schist host rock (andesitic composition) with up to 15% sulphides. The oxidation step is conducted on ore concentrate slurry in an autoclave at 225°C and 3,800 kPa oxygen gas pressure with continuous feed. The slurry takes ca. 1 h to pass through the autoclave, during which time the sulphides are almost completely oxidised. Sulphide oxidation causes strong acidification of the slurry, which is maintained at pH of 1–2 by addition of $CaCO_3$. Scales form on walls in the autoclave, with minerals reflecting progressive oxidation and alteration of the ore through the system. The schist in the ore feed has mineralogy similar to propylitically altered andesite: quartz, albite, muscovite, chlorite, and pyrite. Muscovite undergoes almost complete dissolution, with associated precipitation of quartz and alunite ($KAl_3(SO_4)_2(OH)_6$). Other principal minerals deposited and discharged include anhydrite (and/or gypsum), jarosite ($KFe_3(SO_4)_2(OH)_6$), hematite (and/or amorphous iron oxyhydroxide), and amorphous arsenates. Dissolved ferrous iron passes right through the autoclave, and variably hydrated $Fe^{2+}$and Fe^{3+} sulphate minerals, including rozenite and szomolnokite (both $FeSO_4$.hydrate) and ferricopiapite ($Fe_5(SO_4)_6O(OH)$. hydrate), are formed along the way. The autoclave chemical system resembles acid–sulphate hydrothermal activity in geothermal systems and high-sulphidation epithermal mineral deposits formed in arc environments. These natural acid–sulphate systems are pervaded by volcanic vapours in the near-surface environment, where widespread dissolution of host rocks occurs and deposition of quartz, alunite, and anhydrite is common. Some of the volume loss associated with these natural systems may be due to dissolution of soluble sulphate minerals by later-stage groundwater incursion.

Keywords Hydrothermal · Gold · Andesite · Jarosite · Alunite · Sulphate · High sulphidation

Editorial handling: N. White

D. Craw (✉)
Geology Department, University of Otago,
P.O. Box 56, Dunedin, New Zealand
e-mail: dave.craw@stonebow.otago.ac.nz

Introduction

Acid–sulphate alteration is a result of strong chemical interaction and leaching of rock by hydrothermal fluids in epithermal systems (Stoffregen 1987; Hedenquist et al. 1996, 1998). This style of alteration has a distinctive set of secondary minerals preserved, including alunite and anhydrite (Table 1; Stoffregen 1987; White and Hedenquist 1990; Hedenquist et al. 1996, 2000; Rodgers et al. 2000, 2002; Cooke and Simmons 2000; Simmons et al. 2005). In addition, alteration results in volume loss from host rocks leading to characteristic open cavities in the rock mass. Acid–sulphate alteration occurs in two principal settings in epithermal systems: surficial steam-heated zones (Henley and Ellis 1983; Rodgers et al. 2002) and deeper zones, in which magmatic fluids, particularly vapour, discharge towards the surface (Giggenbach 1992; Hedenquist et al. 1993, 1998). In steam-heated zones, boiling hydrothermal fluids (commonly low-sulphidation epithermal) partition volatile H_2S into the vapour phase, and this oxidises to form sulphuric acid (H_2SO_4) in shallow groundwater (Henley and Ellis 1983; Rye et al. 1992; Rodgers et al. 2000). The resultant warm (ca. 100°C) waters leach soluble material from shallow aquifer rocks, causing meter-scale cavitation and deposition of secondary acid sulphate minerals. In the deeper zones, magmatic fluids exsolve volatile SO_2 that migrates upwards to form sulphurous (H_2SO_3) and suphuric acids at shallower levels (ca. 200–300°C) (Stoffregen 1987; Giggenbach 1992; Hedenquist et al. 1996, 1998). These acids leach the generally andesitic host rocks, which surround the fluid conduits, and facilitate precipitation of acid sulphate minerals (Stoffregen 1987; Hedenquist et al. 1996, 1998). The leaching results in

porous rocks with a framework of less soluble material including quartz, and secondary quartz crystals are deposited in the centimeter-scale cavities (vugs) (Stoffregen 1987; Hedenquist et al. 1996). This style of acid–sulphate alteration is characteristic of high-sulphidation epithermal systems, which can contain economic copper and/or gold (Stoffregen 1987; White and Hedenquist 1990; Hedenquist et al. 1996, 1998). The acid–sulphate alteration zone is surrounded by less intensely altered zones including propylitically altered rocks (Table 1; Hedenquist et al. 1996; Reed1997). This alteration zone represents a transition from relatively reduced, rock-buffered chemical conditions (propylitic) to acid-oxidised conditions (Fig. 1; Giggenbach 1992; Hedenquist et al. 1996).

Pressure-oxidation autoclaves are used to oxidise sulphide minerals so that fine-grained gold is released for cyanidation (Fig. 2a; LaBrooy et al. 1994; Johnstone et al. 2001). A slurry of crushed sulphide-bearing ore is heated under elevated oxygen pressure until the sulphides oxidise (Papangelakis and Demopoulos 1991; LaBrooy et al. 1994). The oxidation reactions are exothermic and the process is self-perpetuating as long as sufficient sulphide minerals and oxygen are supplied (Papangelakis and Demopoulos 1991; LaBrooy et al. 1994). The resulting solutions are acid and rich in sulphate (sulphuric acid). The acid solutions can interact chemically with silicates in the ore in a process that is broadly similar to that of acid sulphate alteration described above. Some of the minerals formed in an autoclave are the same as those found in acid–sulphate alteration zones (Tables 1, 2). This paper presents observations on chemistry and mineralogy in one autoclave as an analogue for acid–sulphate alteration processes in epithermal systems, particularly the deeper zones associated with high-sulphidation systems.

The chemical and mineralogical changes that occur during leaching and cavitation accompanying acid–sulphate alteration are poorly understood because the resulting minerals are removed during the alteration

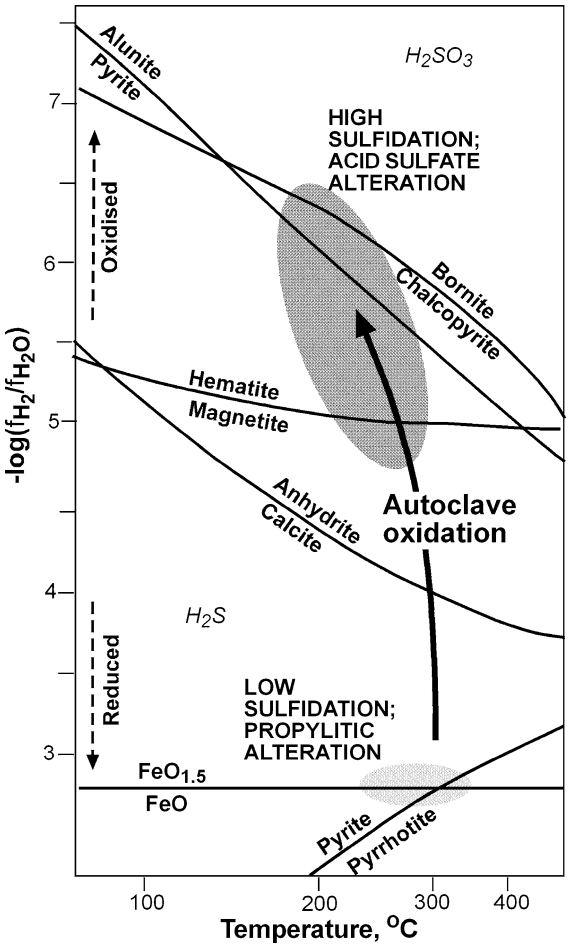

Fig. 1 Temperature-oxidation state diagram for sulphur-rich hydrothermal systems, with oxidation state indicated in terms of hydrogen fugacity ratio in vapour (see text; modified after Giggenbach 1992; Hedenquist et al. 1996). Principal mineral reaction boundaries relevant to epithermal systems are shown with *black lines*. Typical low sulphidation conditions are indicated with *light stipple* (*bottom*), and high sulphidation conditions are indicated with *heavy stipple*. The path of autoclave (and natural system) alteration is indicated with a *heavy arrow*

Table 1 Summary of typical minerals reported from natural hot acid sulphate zones

Alteration zone	Alteration minerals and precipitates	
	Nonmetallic minerals	Metallic minerals
Fumaroles	Amorphous silica, cristobalite, alunite, jarosite, anhydrite (±gypsum), alum, alunogen, aphthitalite (Na sulphate), kaolinite, chlorite	Pyrite, hematite, goethite, Au, Ag, Se, As
Steam-heated ground	Opal, cristobalite, kaolinite, alunite, alunogen, native S	Pyrite, marcasite
High sulphidation propylitic	Quartz, smectite, chlorite, calcite, epidote	Pyrite, pyrrhotite, chalcopyrite, titanite
High sulphidation argillic	Quartz, kaolinite, smectite, illite, sericite	Pyrite, chalcopyrite, rutile
High sulphidation advanced argillic	Quartz, alunite, kaolinite (dickite), pyrophyllite, diaspore, anhydrite	Chalcocite, covellite, bornite, enargite, pyrite, rutile, (hematite, goethite)
High sulphidation ore zone	Residual vuggy quartz, vein quartz, alunite	Pyrite, rutile, Au (±Ag), (hematite, goethite)

Minerals are from Wood (1994), Getahun et al. (1996), Hedenquist et al. (1996, 2000), Cooke and Simmons (2000), Rodgers et al. (2002), Fulignati et al. (2002), Rainbow et al. (2005), and Simmons et al. (2005)

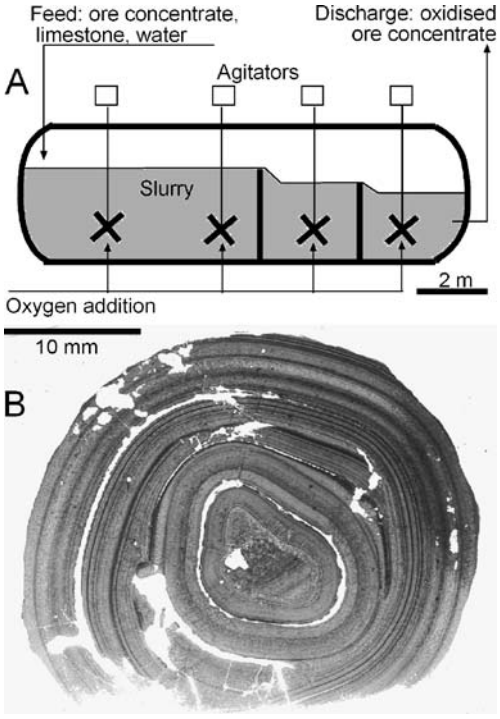

Fig. 2 **a** Sketch of the geometry of the autoclave (after Johnston et al. 2001). A slurry is fed from the left into the first compartment, oxygen is added through the autoclave in each of the three compartments, and oxidised material is discharged from the right. Within the autoclave, the slurry (*grey*) is stirred by agitators (*black crosses*). Scales form on the agitators, walls, and floor of the autoclave. **b** Thin section of a spherical scale ball from the floor of the first compartment, formed concentrically around a fragment of scale (*centre*) that fell from an agitator. *Dark bands* are rich in hematite, and *light bands* are mixtures of rozenite and szomolnokite

process or subsequent water flushing during uplift and erosion. This latter flushing is particularly significant if minerals precipitated during alteration are soluble in more dilute groundwater that infiltrate after alteration has ceased. Hence, natural acid–sulphate zones, by their very nature, are insoluble remnants of more complex mineralogical assemblages. In this study, observations on mineral assemblages are combined with theoretical predictions to provide information for the knowledge gap between acid–sulphate alteration zones at depth and the relict insoluble frameworks that are observed at the surface. The autoclave is essentially an uncontrolled "experiment" on acid–sulphate alteration of andesitic rocks.

General definition of the pressure-oxidation analogue

The autoclave described in this study (Fig. 2a; Johnstone et al. 2001) is located at the Macraes gold mine, New Zealand (Craw 2003). The gold mine is developed in a mesothermal (orogenic) deposit hosted by greenschist facies schist (Craw 2002). The host schist had metasedimentary protoliths with intermediate felsic compositions (Mortimer and Roser 1992). The host rock and primary ore minerals are listed in Fig. 2. These minerals are also characteristic of low fluid/rock ratio propylitic alteration of intermediate volcanic (andesitic) rocks that are common hosts to epithermal systems (Henley and Ellis 1983; White and Hedenquist 1990; Reed 1997). Epidote, a common propylitic alteration mineral (Tables 1 and 2), is abundant in the schist host rocks near Macraes, but the Macraes mineralised zone has epidote altered to siderite and kaolinite, and epidote is rare or absent from the ore. The ore contains abundant hydrothermal graphite (Craw 2002), and is relatively reduced chemically, with oxidation state near to the pyrite–pyrrhotite stability boundary (Fig. 1).

The sulphide content of the ore is typically ca. 1%, and this is concentrated tenfold by flotation of crushed ore. The relative proportions of silicate minerals are changed little by the concentration process. The concentrate is ground to <20 μm before being fed into the autoclave (Fig. 2a) to enhance reactivity. The feed occurs as a slurry of concentrate and low-salinity freshwater (total dissolved solids <500 mg/l) with Na content <50 mg/kg and K content <10 mg/kg. The autoclave has constant temperature of 225°C and >3,000 kPa oxygen gas pressure (Johnstone et al. 2001). The concentrated ore slurry passes through the autoclave in a continuous feed system, and residence time is about 1 h. Oxidation of sulphides, especially pyrite, causes acidification of the slurry throughout the autoclave. Calcite is added to the ore feed to prevent excessive acidification and the slurry in the autoclave has pH <2. Sulphide decomposition is almost total by the time the slurry is discharged, and nearly all sulphur is oxidised to sulphate. However, dissolved Fe^{2+} species persist beyond the autoclave and can take several months to completely oxidise at ambient temperatures (Craw 2003).

Mineral deposits (scales) precipitate and accumulate on the inner walls of the autoclave and on agitators, which stir the slurry as it passes (Fig. 2a; Johnstone et al. 2001). In addition, fragments of scale from the walls or agitators act as nuclei for scale growth on the autoclave floor (Fig. 2b). These scales are detrimental to autoclave efficiency and are removed periodically. However, the scale minerals provide information on phase relations and chemical processes in the autoclave, and these scales are the focus of this study. The scales are generally made up of numerous contrasting monominerallic, biminerallic, and polyminerallic millimeter- to centimeter-thick layers (Fig. 2b), attesting to locally variable chemistry in the slurry. However, there are some general trends in mineralogy through the autoclave and some common coexisting mineral assemblages (Fig. 3). These trends and assemblages have some similarities to those seen in epithermal acid–sulphate systems and form the basis of the discussions below.

Methods and results

Mineral identification

Samples of autoclave scales were obtained when the autoclave was shut down for scale removal. The scales were chipped from exposed surfaces in the autoclave, and

Table 2 Names and formulae for minerals in the autoclave

Autoclave		Model		Epithermal Mineral
Mineral	Formula	Mineral	Formula	
Quartz	SiO_2	Quartz	SiO_2	Quartz[b]
Albite	$NaAlSi_3O_8$			Albite
Phengitic muscovite	$KAl_2Si_3O_{10}(OH)_2$ + Fe, Mg	Annite	$KFe_3Al\ Si_3O_{10}(OH)_2$	Sericite/illite biotite
Fe, Mg chlorite	$Mg_2Fe_3Al_2Si_3O_{10}(OH)_8$	Fe-chlorite	$Fe_5Al_2Si_3O_{10}(OH)_8$	Fe, Mg chlorite epidote
Pyrite	FeS_2	Pyrite	FeS_2	Pyrite[b]
Arsenopyrite	FeAsS	Arsenopyrite	FeAsS	
		Orpiment	As_2S_3	Orpiment/realgar
Chalcopyrite	$CuFeS_2$	Chalcopyrite	$CuFeS_2$	Chalcopyrite
Covellite[a]	CuS	Covellite	CuS	Covellite[b]
		Chalcocite	Cu_2S	Chalcocite[b]
		Bornite	Cu_5FeS_4	Bornite[b]
Hematite, HFO	Fe_2O_3, $Fe(OH)_3$	Hematite	Fe_2O_3	Hematite[b], Goethite[b]
		Saponite	$(e)_{0.33}Mg_3AlSi_3O_{10}(OH)_2.h$	Smectite
		Beidellite	$(e)_{0.33}Al_3Si_3O_{10}(OH)_2.h$	
		Clinoptilolite	$(e)Al_2Si_{10}O_{24}.h$	Zeolites
		Mordenite	$(e)Al_2Si_{10}O_{24}.h$	
		Pyrophyllite	$Al_2Si_4O_{10}(OH)_2$	Pyrophyllite[b]
Alunite	$KAl_3(SO_4)_2(OH)_6$	Alunite	$KAl_3(SO_4)_2(OH)_6$	Alunite[b]
Jarosite	$KFe_3(SO_4)_2(OH)_6$	Jarosite	$KFe_3(SO_4)_2(OH)_6$	Jarosite[b]
		Kaolinite	$Al_2Si_2O_5(OH)_4$	Kaolinite group[b]
		Diaspore	AlO(OH)	Diaspore[b]
Anhydrite	$CaSO_4$	Anhydrite	$CaSO_4$	Anhydrite[b]
Gypsum	$CaSO_4.h$			
Kieserite[a]	$MgSO_4.h$	[Mg sulphate]	$MgSO_4$	
		Mg sulphate (h)	$Mg_3(SO4)_2(OH)_2$	
Mirabilite[a]	$Na_2SO_4.h$	Thenardite	Na_2SO_4	
Felsobanyaite[a]	$Al_4(SO_4)(OH)_{10}.h$			
Szomolnokite	$FeSO_4.h$	[Ferrous sulphate]	$FeSO_4$	
Rozenite	$FeSO_4.h$			
Ferricopiapite[a]	$Fe_5(SO_4)_6O(OH).h$	Ferric sulphate	$Fe_2(SO_4)_3$	
Wustite[a]	FeO			
Claudetite/arsenolite	As_2O_3			
Parasymplesite	$Fe_3(AsO_4)_2.h$			
Scorodite	$FeAsO_4.h$	Scorodite	$FeAsO_4.h$	
Fe-arsenate	Variable			
Ca-arsenate[a]	Variable		$Ca_3(AsO_4)_2$	
		Mg-arsenate	$Mg_3(AsO_4)_2$	
		[Arcanite]	K_2SO_4	
		Hercynite	$FeAl_2O_4$	

Primary minerals are italicised. Also listed are minerals depicted in model phase diagrams (see "Discussion") and observed in hydrothermally altered rocks in epithermal systems. Minerals in brackets did not precipitate in models. *(e)* Exchangeable cation, *h* hydrated, *HFO* hydrated iron oxide. See text for references

[a]Minerals not found in all sampling periods

[b]Acid sulphate alteration mineral

fist-sized specimens were selected from known sites through the autoclave. Similar sets of samples were collected approximately four times a year for 3 years. Fragments (ca. 20–30 g) of samples were ground with an agate mortar and pestle. Resultant powders were mounted for X-ray diffraction (XRD) analysis on glass slides as slurries made with acetone or alcohol. Individual layers were selected from some samples with distinctive layering, and these were analysed separately. The powder mounts were analysed with a Philips PW 1050 diffractometer using Cu Kα radiation. Diffraction patterns were recorded at 1° 2θ/minute, and patterns were recorded digitally. Background stripping, peak indexing, and peak matching were done using software MacDiff, using a comparative database constructed from Joint Committee for Powder Diffraction Studies data.

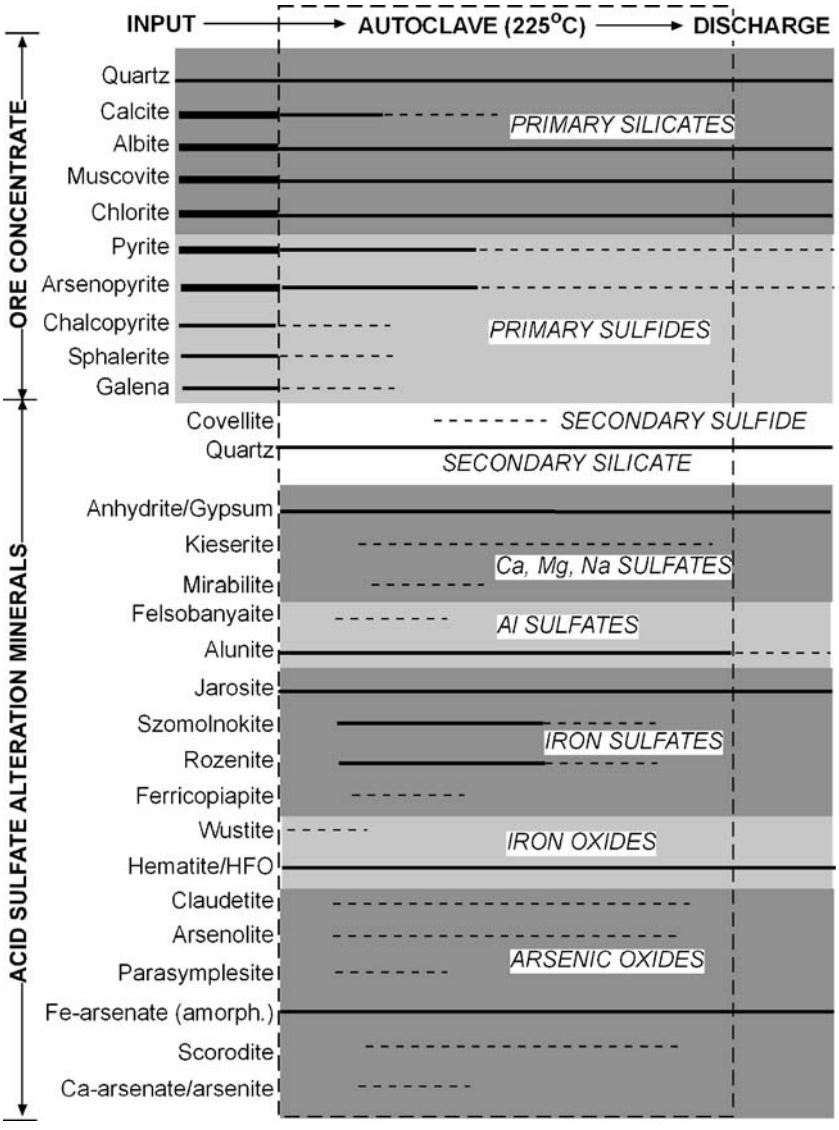

Fig. 3 Distribution of minerals through the autoclave system from the ore slurry input end (*left*) to discharge (*right*). *Heavy lines* denote abundant minerals, *lighter lines* indicate general presence, and *dashed lines* indicate sporadic presence. Primary ore minerals are at the *top* of the diagram, and secondary minerals in the *lower part*. *Shading* links similar mineral groups. *HFO* hydrated iron oxide

Polished thin sections were obtained for samples with equivocal X-ray diffraction results, and some minerals were confirmed optically. Geochemical information on elemental contents of specific layers was obtained by energy-dispersive microprobe analysis using a JEOL 8600 instrument (University of Otago Geology Department). Subsamples (ca. 20 g) of one set of scale samples were analysed by X-ray fluorescence by SpectraChem, Wellington, New Zealand, to determine the principal element concentrations of bulk samples (Fig. 4; Table 3). These analyses are reproducible to within 0.02 wt%. Detection limits for metals are near 1 mg/kg, but all analyses in Table 3 are quoted as weight percent to two decimal places for ease of comparison of the major chemical constituents of the scales. The additional chemical data assisted in confirming some X-ray diffraction mineral identifications. Some scale samples contained X-ray amorphous material, and this was identified in a general way with the geochemical techniques.

Minerals identified in scales are summarised in Table 2 and their relative positions in the autoclave are depicted in Fig. 3. The most abundant minerals are indicated with heavy black lines in Fig. 3, and subordinate minerals are shown with dashed lines. The general order of occurrence of minerals through the autoclave was consistent in all sampling periods, and this is summarised in Fig. 3 also. However, the degree of overlap through the autoclave of some mineral occurrences varied slightly between sampling periods.

The scales were dominated by calcium minerals (mainly anhydrite, Fig. 3) at the input end of the autoclave, as shown by bulk chemical analyses (Table 3, Fig. 4a,b). The proportion of calcium-bearing scale minerals generally decreased through the autoclave (Fig. 3a), and silica became predominant towards the output end, as secondary quartz formed (Figs. 3 and 4a). Likewise, iron content of scales showed a general increase through the autoclave, although these iron concentrations were widely variable, reflecting irregular occurrences of jarosite, hematite, and scorodite or amorphous Fe-arsenate (Figs. 3 and 4b). The hematite in the autoclave is crystalline with well-defined X-ray diffraction peaks, but hydrated iron oxide (HFO) in

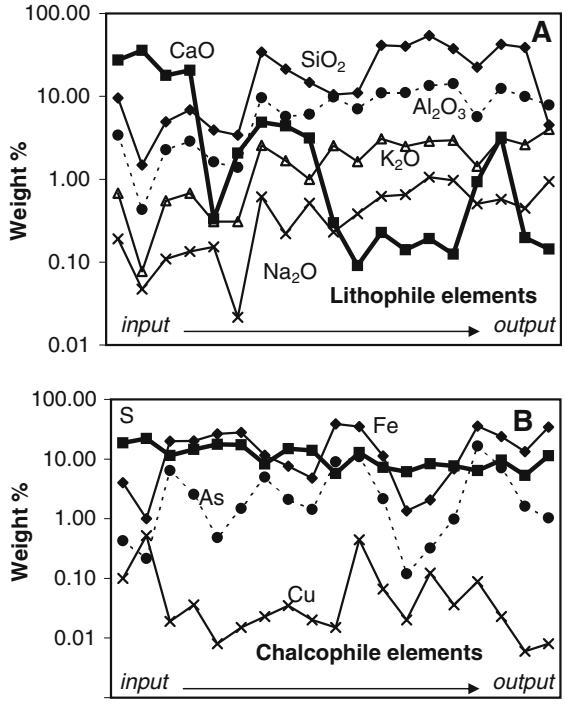

Fig. 4 Chemical composition of scales through the autoclave (Table 2). **a** Lithophile elements. **b** Chalcophile elements

the discharge material is amorphous or poorly crystalline two-line ferrihydrite. The low Na content of the alunite/jarosite-bearing scales (Fig. 3, Table 3) suggests that jarosite and alunite have little Na in solid solution (cf. natrojarosite scale reported by Whittington and Muir 2000).

Scale arsenic concentration variations were independent of iron at the input end but varied in sympathy with iron towards the discharge end as the Fe-arsenates became more prevalent (Fig. 4b). Potassium and aluminium contents of scales increased steadily through the autoclave as alunite became volumetrically more important (Figs. 3 and 4a). Sodium content of scales was minor and variable through the autoclave (Fig. 4a; Table 3). Copper was generally low in scales but locally elevated as minor covellite formed (Figs. 3 and 4b).

Phase diagrams

Mineral phase relationships were modelled using ACT2 from the Geochemists Workbench software package (Bethke 1998). Modelling was done at 200°C because the software thermodynamic database was more complete at this temperature than at 225°C. Revised arsenopyrite stability data from Pokrovski et al. (2002) were incorporated into the phase diagrams. Phase diagrams were constructed for geochemical subsystems for simplicity, using three to six dissolved species at a time (Figs. 5 and 6). Model concentrations of dissolved species were assumed to be high (generally 0.1 mol/l). Relative concentrations of some species were varied to obtain realistic phase diagrams, with reference to observed assemblages. The intimate interlayering of different minerals in the scales suggests that equilibrium was not attained at each stage through the autoclave. For example, the alternating layers of ferrous sulphates (low Fe^{+++}/Fe^{++}) and hematite (high Fe^{+++}/Fe^{++}) in the scale in Fig. 2b shows that redox states fluctuated over a wide range at that site on a scale of hours or days. Hence, no attempts have been made to construct detailed equilibrium models. Instead, model phase diagrams were compiled to encompass the generally observed phases and phase relationships through the autoclave.

Many of the sulphate minerals identified at room temperature are hydrated, whereas minerals depicted in the phase diagrams at 200°C are not (Table 2). At least some of this hydration has occurred during cooling of the autoclave and subsequent sample storage, transport, and preparation, so the anhydrous minerals are more representative of high temperature conditions. Highly soluble mineral species of aluminium sulphate, magnesium sulphate, and ferrous sulphate that occur in the autoclave scales are depicted as aqueous species (e.g. $FeSO_4^0$). The crystalline forms in the scales precipitated as concentrated solutions evaporated in the autoclave during ore processing or during cooling and evacuation for descaling.

Axes on the phase diagrams were selected to show the significance of some key parameters for mineral stability, especially pH and progressive oxidation (ferric/ferrous ratio) that are an essential feature of the autoclave process. Concentrations of principal cations are used as axes in some diagrams to show the significance of variations of these parameters to mineral occurrences. The variety of minerals that occur intimately interlayered with each other shows that these cations varied widely in concentration on the millimeter scale as the scales built up.

Reaction modelling

Progressive reaction of key minerals in the autoclave was modelled using the program REACT, a part of the Geochemists Workbench package (above). Results for model runs were plotted using GTPLOT, another program in the same package, in terms of amounts of minerals reacted (grams of muscovite reacted in Fig. 7a–d) and amounts of minerals present at any stage along this reaction path (grams of minerals present in Fig. 7a–d). Models assumed a constant pH of 2, and constant fugacity of oxygen gas of 1. Initial solution compositions had nominal concentrations of Na^+, K^+, Ca^{++}, Mg^{++}, Cl^-, HCO_3^- of 10 mg/kg, and Al^{+++} and SiO_2(aq) of 0.001 mg/kg, and these are representative of the low-salinity input water for the autoclave (above). Initial Fe^{++} and SO_4^{--} of 0.1 mol/l, combined with the low pH, represented a system that had already undergone pyrite oxidation.

Results of the modelling runs were sensitive to amounts and proportions of minerals reacted. Amounts and proportions were chosen based on observed concentrate mineralogy, with differing proportions run to test sensitivity to

Table 3 X-ray fluorescence analyses of lithophile and chalcophile elements in autoclave scales

Lithophile elements

Sample	SiO_2	TiO_2	Al_2O_3	MgO	CaO	Na_2O	K_2O	P_2O_5
1	9.53	0.22	3.40	1.00	27.31	0.19	0.68	0.04
2	1.48	0.06	0.43	0.21	35.87	0.05	0.08	0.00
3	4.94	0.15	2.27	0.00	17.85	0.11	0.55	0.12
4	6.84	0.20	2.87	0.00	20.64	0.13	0.68	0.25
5	3.93	0.18	1.62	4.60	0.33	0.15	0.31	0.07
6	3.40	0.19	1.38	3.70	2.07	0.02	0.31	0.08
7	34.27	1.62	9.63	1.03	4.87	0.61	2.57	0.22
8	21.29	1.11	5.74	1.33	4.41	0.22	1.68	0.12
9	14.75	1.02	6.09	0.76	3.15	0.51	1.00	0.10
10	10.50	0.28	9.80	0.00	0.30	0.23	2.55	0.55
11	11.03	0.23	7.04	1.83	0.09	0.38	1.63	0.55
12	41.43	2.03	11.00	0.00	0.23	0.62	3.08	0.36
13	40.18	1.75	11.08	0.06	0.14	0.65	2.49	0.13
14	54.09	1.26	13.52	0.07	0.19	1.06	2.88	0.06
15	37.69	0.88	14.23	0.00	0.12	0.97	2.95	0.04
16	22.55	0.93	5.66	0.00	0.93	0.50	1.44	0.33
17	42.37	1.98	12.42	0.00	3.20	0.57	3.13	0.20
18	38.84	1.62	9.98	0.00	0.20	0.45	2.62	0.11
19	4.51	0.10	7.86	0.00	0.14	0.94	4.00	0.03

Chalcophile elements

Sample	Mn	Fe	Cu	Zn	As	S
1	0.10	4.02	0.10	0.04	0.43	18.72
2	0.15	1.00	0.52	0.01	0.22	22.21
3	0.03	19.97	0.02	0.03	6.43	11.44
4	0.03	20.06	0.04	0.04	2.56	14.53
5	0.31	26.33	0.01	0.29	0.48	17.69
6	0.30	27.84	0.02	0.27	1.49	17.33
7	0.03	11.62	0.02	0.07	4.99	8.23
8	0.03	7.58	0.04	0.05	2.09	14.84
9	0.02	4.80	0.02	0.03	1.43	13.92
10	0.01	38.91	0.02	0.05	8.96	5.71
11	0.12	35.03	0.44	0.16	10.97	12.88
12	0.00	11.31	0.07	0.01	2.16	7.24
13	0.00	1.35	0.02	0.00	0.12	6.12
14	0.00	2.06	0.12	0.00	0.32	8.38
15	0.00	6.85	0.04	0.00	0.98	7.65
16	0.04	35.54	0.09	0.11	16.49	6.43
17	0.02	23.76	0.02	0.07	7.13	9.64
18	0.00	13.34	0.01	0.00	1.62	5.33
19	0.00	34.30	0.01	0.00	1.03	11.32

Sample numbers represent sampling order through the autoclave from input area (1) to output area (19)

variations. Model reactions depicted in Fig. 7a–d involve the most reactive feed minerals and the minerals most relevant to this study (Table 2).

Discussion

Comparison to natural acid–sulphate alteration

Most of the common minerals recognised in natural acid–sulphate alteration zones (Tables 1 and 2) are found in the autoclave scales described in this study. Some key minerals, such as alunite, anhydrite, and oxidised copper sulphide (Fig. 1), which distinguish hypogene high-sulphidation alteration from low-sulphidation processes (Hedenquist et al. 1996, 2000; Cooke and Simmons 2000), all occur in close proximity in the autoclave (Fig. 3; Tables 1 and 2). These minerals form as a direct result of acid–sulphate alteration of rock of andesitic composition in relatively oxidised fluids in both autoclave and hypogene high-sulphidation hydrothermal systems. Likewise, alunite and anhydrite are common constituents of acid sulphate

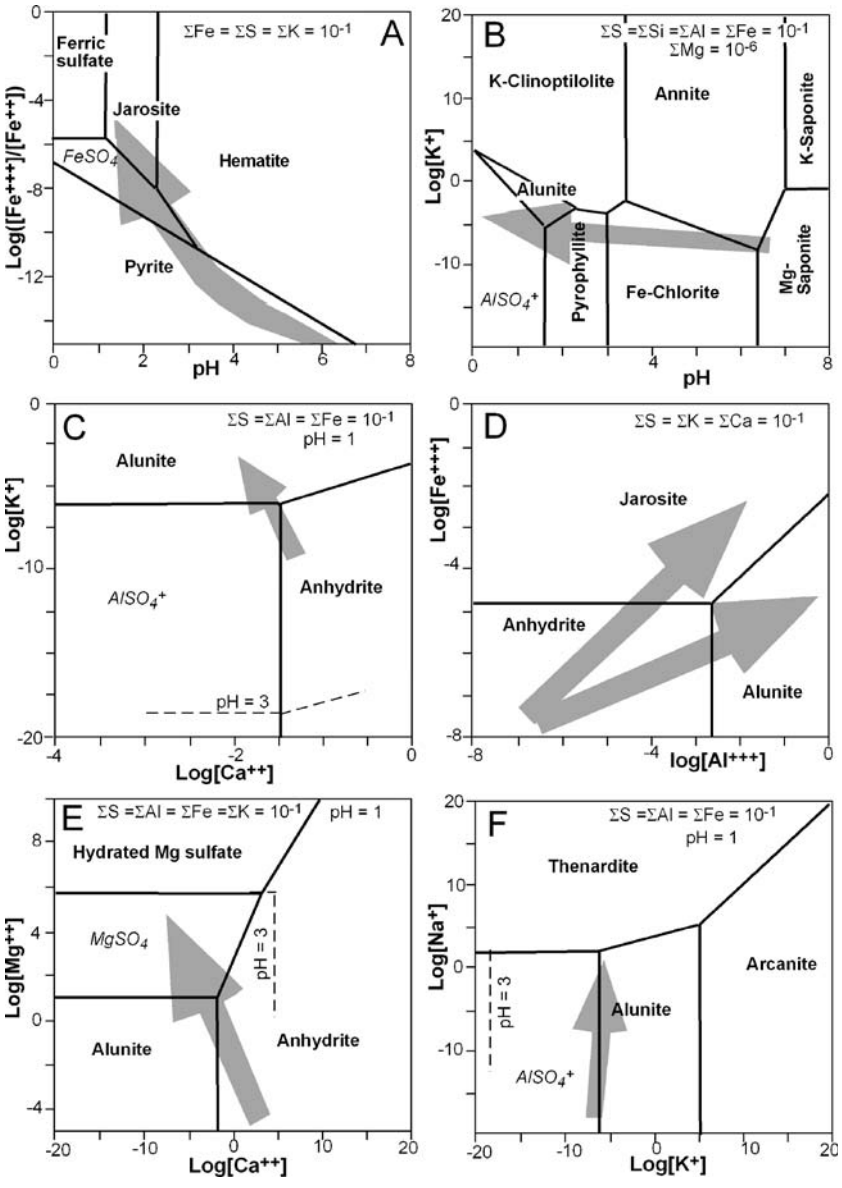

Fig. 5 Phase diagrams for principal autoclave minerals relevant to acid-sulphate alteration calculated using Geochemists Workbench for autoclave solutions at 200°C with compositions indicated on the diagrams. *Grey arrows* indicate typical reaction pathways deduced for autoclave reactions. See text for description of individual diagrams and pathways

fumarole deposits on volcanic edifices (Table 1; Wood 1994; Getahun et al. 1996; Fulignati et al. 2002).

Hematite and/or HFO are common in the autoclave scales, especially in the downstream part of the system (Fig. 3). Hematite and/or goethite occur in natural fumarole deposits (Table 1), but are not common in hypogene high-sulphidation systems where pyrite predominates (Hedenquist et al. 1996, 2000; Cooke and Simmons 2000). Hematite and goethite are reported from the Pierina deposit, a Peruvian hypogene high-sulphidation system, but these minerals are thought to have formed in the latter stages of the paragenesis after incursion of meteoric water (Rainbow et al. 2005). The autoclave alteration process apparently mimics the most oxidised parts of acid–sulphate alteration systems and is more oxidised than typical hypogene high-sulphidation hydrothermal activity. Acid–sulphate alteration associated with steam-heated ground at the water table above low-sulphidation hydrothermal systems also occurs under redox conditions too low for hematite or HFO formation and pyrite occurs instead (Table 1; Fig. 1). Subsequent oxidation of pyrite above the water table can lead to the formation of goethite and/or jarosite (Rodgers et al. 2000, 2002; Simmons et al. 2005).

Quartz is the only silicate formed in the autoclave, and quartz is a common constituent of the scales through the whole system (Fig. 3). This quartz is fully crystalline, in contrast to variably crystalline silica minerals that occur, along with cristobalite, in fumarole deposits (Table 1). Crystalline quartz is also a common constituent of propylitic, argillic, and advanced argillic alteration zones in hypogene high-sulphidation hydrothermal systems (Table 1). However, vein quartz is less common in the ore zones of these hypogene acid–sulphate alteration zones, where vuggy residual quartz is one of the most distinctive features (Table 1; Hedenquist et al. 1996, 2000; Cooke and Simmons 2000). Residual quartz undoubtedly occurs in the autoclave as well, but this is not represented in the scales and is discharged with the slurry (Fig. 2a). Other

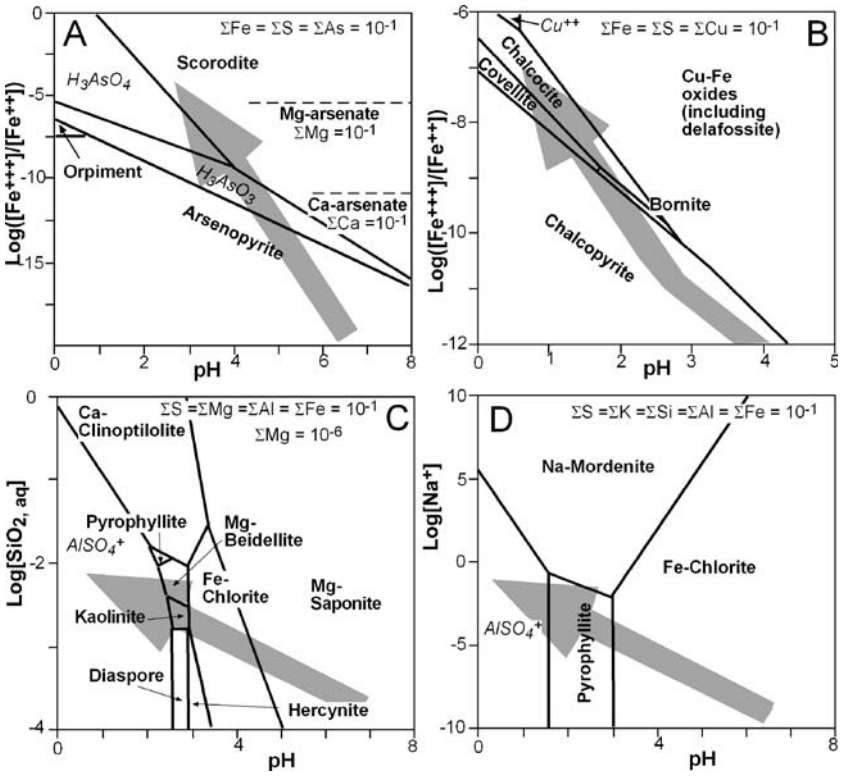

Fig. 6 Phase diagrams for minor components of the autoclave system calculated using Geochemists Workbench for autoclave solutions at 200°C with compositions indicated on the diagrams. *Grey arrows* indicate typical reaction pathways deduced for autoclave reactions. See text for description of individual diagrams and pathways

silicates, such as smectites, kaolinite or dickite, and pyrophyllite, which form in many natural acid–sulphate zones (Table 1), have not precipitated in the autoclave scales, and this observation is further investigated via reaction modelling (below).

It is clear from the autoclave scale mineralogy (Table 2) that numerous sulphate minerals can form under acid–sulphate alteration conditions but are rare or absent from natural acid–sulphate alteration zones. These sulphate minerals may have formed in natural acid–sulphate zones during initial alteration, but may have since been removed in solution in later waters because of their high solubility. This dissolution of soluble sulphate minerals may be responsible for the extensive open cavities that characterise most natural acid–sulphate alteration zones. The exact mineralogical nature of these now-dissolved species is

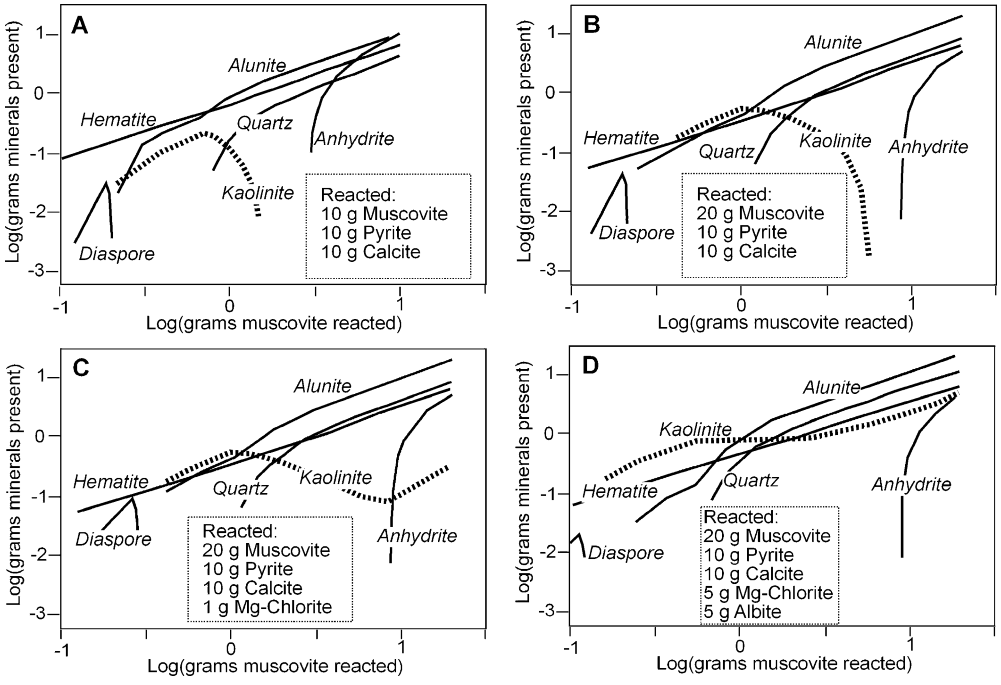

Fig. 7 Reaction progress diagrams, calculated using Geochemists Workbench, for autoclave decomposition of key ore feed minerals. Note *logarithmic scales* on both axes. Reaction progress (*horizontal axis*) is depicted in terms of amount (grams) of initial muscovite (indicated in each diagram) that has been consumed. Amount of each indicated mineral present at each stage through the reaction is indicated on the *vertical scale*. *Lines* with positive slopes show minerals forming, and negative slopes show mineral consumption. See text for description of individual diagrams

difficult to determine, as even in the autoclave situation they rapidly become variably hydrated before analysis (Table 2). Transient occurrences of Al and Na sulphate minerals in some surface fumarole deposits (Table 1) attest to the potential for formation of such minerals throughout acid–sulphate alteration zones.

Arsenic minerals are not as abundant in natural acid–sulphate systems as they are in the autoclave (Table 1). The autoclave is too oxidised for formation of arsenic sulphides, such as orpiment, realgar, or enargite, that occur in natural hydrothermal systems (Table 2), and arsenates form instead (Fig. 3). The oxidised arsenic minerals formed in the autoclave (Fig. 3) are all readily soluble in dilute solutions, and it is possible that these arsenic minerals do form in relatively oxidised acid–sulphate alteration zones (with hematite and/or goethite; see above) and are removed by later groundwaters.

Mineral relationships

Despite the widespread interlayering of different minerals in scales and associated disequilibrium in the autoclave, there are some general mineralogical trends through the autoclave system (Fig. 3). These trends are mainly associated with progressive oxidation and acidification, but products of oxidation reactions also facilitate other reactions and mineral deposition through the autoclave. Some possible geochemical trends in the autoclave with associated mineral paragenetic sequence are indicated with grey arrows in Figs. 5 and 6. These paragenetic sequences may have some significance to paragenetic sequences in natural acid–sulphate alteration zones, as discussed below.

Bulk chemical analyses (Table 3) show that Fe, S, Ca, K and Al were important elements, and relationships amongst some relevant minerals involving these elements are shown in Fig. 5a–c. Oxidation of pyrite is one of the most prominent reactions in the autoclave, and this initially yields an acid solution rich in dissolved ferrous sulphate:

$$pyrite + 3.5O_{2(g)} + H_2O \Rightarrow FeSO_{4(aq)} + SO_4^{2-} + 2H^+ \quad (1)$$

Partial oxidation of dissolved ferrous iron results in precipitation of ferric sulphate, jarosite, and/or hematite (Fig. 5a). The importance of the dissolved ferrous sulphate stage is demonstrated by the common occurrences of rozenite and/or szomolnokite (Table 2; Fig. 3) and the persistence of unoxidised Fe^{2+} in autoclave discharge waters (Craw 2003). This persistence of Fe^{2+} in the solution, despite extensive oxidation, may explain why pyrite is the dominant metallic mineral in most natural acid–sulphate systems rather than hematite (Table 1). Intimate interlayering of Fe^{2+} sulphates and hematite in the autoclave (Fig. 2b) shows that only minor changes in the environment are needed to induce precipitation of minerals of different oxidation states.

Acid from pyrite oxidation causes decomposition of the phyllosilicates chlorite and phengitic muscovite (depicted as annite in the model, Fig. 5b), releasing Al^{3+} and K^+ into solution. Most potassium recombines with aluminium to form alunite from the sulphate-rich solution (Fig. 5b,c):

$$muscovite + chlorite + 9SO_4^{2-} + 20H^+ \Rightarrow alunite + 6quartz + 2MgSO_{4(aq)} + 3FeSO_{4(aq)} + 2AlSO_4^+ + 12H_2O \quad (2)$$

The above reactions reflect the processes of progressive alteration of andesitic rock from propylitic to advanced argillic alteration in natural acid–sulphate systems (Table 1).

Some potassium from muscovite decomposition goes to form jarosite in association with ferric sulphate and hematite (Fig. 5a). Alunite and jarosite formation is locally inhibited by high Ca^{2+} released by dissolution of calcite near the autoclave input end and abundant anhydrite precipitates (Figs. 3, 4a and 5c,d). Alunite is the dominant potassium sulphate mineral because of high dissolved Al^{3+} from decomposition of phyllosilicates (Eq. 2). Dissolved Fe^{3+} is generally relatively low compared to Al^{3+}, as hematite and ferric sulphate precipitate (Fig. 5a) and much dissolved Fe^{2+} (Eqs. 1 and 2) fails to oxidise (above). Hence, jarosite is less common than alunite, although some samples contain both sulphate minerals intergrown. The relationships between these sulphate minerals are depicted in Fig. 5d. This may explain why alunite is the dominant sulphate in natural acid–sulphate alteration systems (Table 1). There may be some solid solution between jarosite (Fe-rich) and alunite (Al-rich), as described in similar autoclave scales by Whittington and Muir (2000). However, these minerals show distinctly different XRD patterns in the Macraes autoclave scales and in natural acid–sulphate systems (Hedenquist et al. 1996, 2000; Cooke and Simmons 2000), and both minerals can be identified separately in some individual autoclave samples.

Locally high concentrations of dissolved Mg from Eq. 2 results in minor deposition of magnesium sulphate minerals instead of alunite in the middle of the autoclave (Table 2; Figs. 3 and 5e), but high Ca^{++} near the autoclave input ensures the predominance of anhydrite irrespective of Mg^{++} content (Fig. 5e). Hence, Mg^{++} derived from natural acid–sulphate alteration of, e.g. chlorite (Table 1), is unlikely to result in deposition of Mg sulphates in natural systems. Dissolved sodium generated from decomposition of albite (Table 2) is sufficiently high locally in the autoclave to allow precipitation of sodium sulphate rather than alunite (Fig. 5f). Natural Na-bearing sulphates form instead of alunite in an acid sulphate fumarole on Mt. St. Augustine volcano, Alaska (Getahun et al. 1996).

Decomposition of arsenopyrite under acid conditions does not contribute directly to acidity, but it does contribute

to the high sulphate in the autoclave and high dissolved arsenate:

$$arsenopyrite + 1.5H_2O + 3.25O_{2(g)} \Rightarrow FeSO_{4(aq)} + H_3AsO_{4(aq)} \quad (3)$$

Oxidation of the ferrous iron could generate some additional acidity as well. The dissolved arsenic combines with available Fe^{3+} to form amorphous Fe-arsenate and/or scorodite (Fig. 3; Table 2). This reaction occurs only at relatively high pH (>2 in Fig. 6a), and the arsenic remains in solution under more acid conditions (Fig. 6a). Calcium arsenate minerals are rare in the autoclave (Fig. 3) and are stable under near-neutral pH conditions (Fig. 6a) that are also rare in the autoclave. Magnesium arsenate has a broader pH stability range than Ca-arsenate (Fig. 6a) but has not yet been detected in the autoclave. Arsenates are not reported from natural acid–sulphate systems (Table 1) but may have been removed by late stage groundwater (see above).

Oxidation of the minor chalcopyrite present occurs throughout the autoclave, and little deposition of copper minerals occurs. Most copper passes through the autoclave in solution as either Cu^{+} or Cu^{2+} under oxidised low pH conditions (Fig. 6b). However, minor localised deposition of covellite has occurred (Fig. 3; Tables 2 and 3), as predicted by the geochemical model (Fig. 6b). This model predicts a sequence of copper sulphides from chalcopyrite through bornite to covellite and chalcocite, similar to that observed with progressive alteration in natural hypogene high-sulphidation systems (Table 1).

Silicate minerals

Silicates other than quartz are notably absent from the autoclave scales (Table 2). Zeolites such as clinoptilolite and mordenite, and clay minerals such as kaolinite, pyrophyllite, beidellite and saponite (Tables 1 and 2) are theoretically stable in equilibrium with solutions with high dissolved silica (Fig. 5c,d), and these occur in natural hydrothermal alteration systems (Tables 1 and 2). However, these silicate minerals are stable at relatively high pH (>2), and decompose to yield dissolved Al sulphate at lower pH (Fig. 5c,d). Furthermore, quartz precipitates when dissolved silica reaches $>10^{-3}$ mols/kg (Fournier 1985), maintaining dissolved silica concentrations at or below this level. In addition, most silicate minerals formed in acid–sulphate alteration zones are replacement phenomena, after pre-existing silicates such as feldspar, chlorite, and muscovite, at lower water/rock ratios than the main alteration zone (Reed 1997). In contrast, autoclave scale deposition occurs from the solution after the primary silicates have been mostly dissolved at low pH.

Dissolution of silicates in the autoclave is depicted by the progressive reaction models (Fig. 7a–d). Reaction of equal quantities of pyrite, calcite and muscovite yields the most common scale minerals alunite, anhydrite, quartz and hematite (Fig. 7a). Kaolinite forms early in the model, but then redissolves to yield quartz and more alunite (Fig. 7a). Doubling the total amount of muscovite does not change the overall pattern of the progressive reaction system, although kaolinite persists to later stages (Fig. 7b). The model in Fig. 7b has the highest proportion of muscovite likely to occur in the concentrate ore feed to the autoclave, so if muscovite is the only reacting Al mineral, kaolinite will not survive progressive reaction. Initial precipitation of kaolinite, followed by later dissolution is similar to progressive alteration in natural hypogene high-sulphidation systems where kaolinite occurs in argillic alteration zones but is absent from the highly leached ore zone (Table 1).

Addition of Al-rich minerals such as chlorite and albite to the reaction system results in re-emergence of kaolinite as a precipitating mineral in the latter stages of the reaction (Fig. 7c,d). Only trace amounts of kaolinite precipitate when the proportion of chlorite is small (5% of muscovite component; Fig. 7c). However, when moderate amounts of chlorite and albite are reacted, kaolinite becomes an important reaction product at the end of progressive reaction (Fig. 7d), as in argillic alteration zones (Table 1). Diaspore, a common acid sulphate mineral (Tables 1 and 2) is an early formed mineral in all the models in Fig. 7a–d, but this rapidly redissolves, and is not seen in autoclave scales. Diaspore forms in natural advanced argillic alteration zones, but has been redissolved from the residual vuggy quartz ore zones (Table 1), in a similar manner to that described by the models in Fig 7a–d.

Conclusions

Pressure-oxidation in an autoclave at the Macraes gold mine, New Zealand, provides a useful analogue for natural acid–sulphate alteration of andesitic rocks associated with epithermal mineralisation processes. Sulphide oxidation in the autoclave, at 225°C, causes acidification of ore slurry to pH of <2, and these conditions are similar to those deduced for natural systems. Scales on walls in the autoclave contain minerals reflecting progressive oxidation and alteration of the ore through the system, and many of these minerals are also observed in natural acid–sulphate systems. Schist in the ore feed has mineralogy similar to propylitically altered andesite found in epithermal systems. Muscovite undergoes almost complete dissolution, with associated precipitation of quartz and alunite. Abundant anhydrite and/or gypsum form initially, as calcite is added to limit acidification. Jarosite, hematite (and/or amorphous iron oxyhydroxide) and amorphous arsenates are the other principal scale minerals. Oxidation is not complete in the autoclave, and dissolved ferrous iron passes right through. Several Fe^{2+} and Fe^{3+} sulphate minerals, including rozenite, szomolnokite, and ferricopiapite, form through the autoclave. Kaolinite and diaspore were not observed in the autoclave, and geochemical modelling predicts that these early-formed minerals should redissolve. The autoclave chemical system resembles that inferred for acid–

sulphate hydrothermal activity in high-sulphidation epithermal mineral deposits formed in volcanic arc environments. One of the characteristics of these systems is volume loss that accompanies alteration and mineralisation, leaving a remnant quartz–alunite alteration assemblage with abundant open cavities. Some of the volume loss associated with these natural systems may be due to dissolution by later-stage groundwater of soluble sulphate minerals of the type observed in this study. In particular, soluble Fe^{2+} sulphates may form from a hydrothermal fluid that has ferrous iron as the dominant Fe species despite the relatively high-oxidation state. Observations of the autoclave scales suggest that minor and localised (centimeter scale) variations in solution chemistry can readily change equilibrium mineral phases being deposited and the mineral phase successions that occur with progressive oxidation.

Acknowledgements Financial support for this study was provided by University of Otago and Oceana Gold (NZ) Ltd. Logistical support for sampling, and frequent useful discussions, were provided by the Oceana staff, particularly Brent Hill, Quenton Johnston, and Steve LaBrooy. Expert laboratory assistance was provided by Damian Walls and Dusk Mains. Helpful comments on the manuscript by Larry Meinert and reviewers David Cooke and James MacDonald resulted in substantial improvement in the presentation.

References

Bethke CM (1998) The geochemist's workbench, Release 3.0, University of Illinois, USA

Cooke DR, Simmons SF (2000) Characteristics and genesis of epithermal gold deposits. In: Hagemann SG, Brown PE (eds) Gold in 2000. Rev Econ Geol 13:221–244

Craw D (2002) Geochemistry of late metamorphic hydrothermal alteration and graphitisation of host rock, Macraes gold mine, Otago Schist, New Zealand. Chem Geol 191:257–275

Craw D (2003) Geochemical changes in mine tailings during a transition to pressure-oxidation process discharge, Macraes Mine, New Zealand. J Geochem Explor 80:81–94

Fournier RO (1985) Behaviour of silica in hydrothermal systems. In: Berger BR, Bethke PM (eds) Geology and geochemistry of epithermal systems. Rev Econ Geol 2:45–62

Getahun A, Reed MH, Symonds R (1996) Mount St. Augustine volcano fumarole wall rock alteration: mineralogy, zoning, composition and numerical models of its formation process. J Volcan Geotherm Res 71:73–107

Giggenbach WF (1992) Magma degassing and mineral deposition in hydrothermal systems along convergent plate boundaries. Econ Geol 87:1927–1944

Fulignati P, Sbrana A, Luperini W, Greco V (2002) Formation of rock coatings induced by the acid fumarole plume of the passively degassing volcano of La Fossa (Vulcano Island, Italy). J Volcan Geotherm Res 115:397–410

Hedenquist JW, Simmons SF, Giggenbach WF, Eldridge CS (1993) White Island, New Zealand, volcanic-hydrothermal system represents the geochemical environment of high-sulfidation Cu and Au ore deposition. Geology 21:731–734

Hedenquist JW, Izawa E, Arribas A, White NC (1996) Epithermal gold deposits: styles, characteristics, and exploration. Society of Resource Geology Special Publication 1, p 16

Hedenquist JW, Arribas A, Reynolds TJ (1998) Evolution of an intrusion-centered hydrothermal system: far Southeast Lepanto porphyry and epithermal Cu–Au deposits, Phillipines. Econ Geol 93:373–404

Hedenquist JW, Arribas AR, Gonzalez-Urien E (2000) Exploration for epithermal gold deposits. In: Hagemann SG, Brown PE (eds) Gold in 2000. Rev Econ Geol 13:245–277

Henley RW, Ellis AJ (1983) Geothermal systems ancient and modern: a geochemical review. Earth Sci Rev 19:1–50

Johnstone Q, LaBrooy S, Craw D (2001) Formation and remediation of scales, pressure oxidation plant, Macraes Mine, New Zealand. Proceedings Aus Inst Min Metall NZ Branch 34th Ann Conf, pp 275–280

LaBrooy SR, Linge HG, Walker GS (1994). Review of gold-extraction from ores. Miner Eng 7:1213–1241

Mortimer N, Roser BP (1992) Geochemical evidence for the position of the Caples-Torlesse boundary in the Otago Schist, New Zealand. J Geol Soc (Lond) 149:967–977

Papangelakis VG, Demopoulos GP (1991) Acid pressure-oxidation of pyrite: reaction kinetics. Hydrometallurgy 26:309–325

Pokrovski GS, Kara S, Roux J (2002) Stability and solubility of arsenopyrite, FeAsS, in crustal fluids. Geochim Cosmochim Acta 66:2361–2378

Rainbow A, Clark AH, Kyser TK, Gaboury F, Hodgson CJ (2005) The Pierina epithermal Au–Ag deposit, Ancash, Peru: paragenetic relationships, alunite textures, and stable isotope geochemistry. Chem Geol 215:235–252

Reed MH (1997) Hydrothermal alteration and its relationship to ore fluid composition. In: HL Barnes (ed) Geochemistry of hydrothermal ore deposits. Wiley, New York, pp 303–366

Rodgers KA, Hamlin KA, Browne PRL, Campbell KA, Martin R (2000) The steam condensate alteration mineralogy of Ruatapu cave, Orakei Korako geothermal field, Taupo Volcanic Zone, New Zealand. Min Mag (Lond) 64:125–142

Rodgers KA, Cook KL, Browne PRL, Campbell KA (2002) The mineralogy, texture and significance of silica derived from alteration by steam condensate in three New Zealand geothermal fields. Clay Miner 37:299–322

Rye RO, Bethke PM, Wasserman MD (1992) The stable isotope geochemistry of acid sulfate alteration. Econ Geol 87:225–262

Simmons SF, White NC, John DA (2005) Geological characteristics of epithermal precious and base metal deposits. In: Hedenquist, JW, Thompson JFH, Goldfarb RJ, Richards JP (eds) Econ Geol 100th Anniv Vol, pp 485–522

Stoffregen RE (1987) Genesis of acid-sulfate alteration and Au–Cu–Ag mineralization at Summittville, Colorado. Econ Geol 82:1575–1591

White NC, Hedenquist JW (1990) Epithermal environments and styles of mineralization: Variations and their causes, and guidelines for exploration. J Geochem Explor 36:445–474

Whittington BI, Muir D (2000) Pressure acid leaching of nickel laterites: a review. Min Proc Ext Met Rev 21:527–600

Wood CP (1994) Mineralogy at the magma-hydrothermal system interface in andesite volcanoes, New Zealand. Geology 22: 75–78